Research on Wake Characteristics of Wind Turbines in Mountainous Terrain

Guoliang Zhao

Central South Electric Power Test & Research Institute of China Datang Corporation Science and Technology Research Institute Co., Ltd, Zhengzhou, China

Abstract

For mountain-complex terrain conditions, turbine wake velocity profiles are jointly modulated by topographic relief and incoming-flow wind features, which breaks the uniform wake distribution pattern and imposes substantial impacts on the wind-energy capture performance of downstream wind turbines. To reveal the wake evolution mechanism for wind farms located in mountainous zones, this paper adopts field LiDAR measurement datasets to quantify how terrain conditions and incoming-flow properties govern wake development tendencies. The test results demonstrate that wind-shear effects produce obvious asymmetry for wind-speed fields within the wake region. Topographic undulations create successive elevation variations along the wake propagation path, which drives the downward offset of wake core; further, the downward-offset magnitude of wake core presents an approximate linear correlation with local terrain elevation difference.

Keywords

Wake evolution, mountain-zone wake characteristics, mountainous wind farm.

1. Introduction

When oncoming airflow passes through a wind turbine rotor, the downstream flow will experience velocity deficit together with amplified turbulence intensity, and such physical phenomenon is defined as the turbine wake effect. For large-scale wind farms, power output losses induced by turbine wake interference can reach 10%-20% of total generation [1-2].

As onshore wind projects over flat terrains have been largely exploited, mountainous high-altitude regions rich in wind resources have become key targets for wind-farm micro-siting. Combined influences from wind-shear effect [3] (i.e., vertical wind-speed gradient before turbine rotor plane) and rugged terrain undulation [4] form highly complicated wake flow fields inside mountain wind farms, which significantly increases the difficulty of precise micro-siting work. Accordingly, investigating wake behaviours under coupled actions of wind shear, topographic features and incoming-flow parameters (inflow wind speed, incoming turbulence intensity) carries practical engineering value for mitigating wake interference and boosting the power production of mountain wind farms.

Light detection and ranging (LiDAR) technique has emerged as a powerful experimental tool for wake-feature observation and has yielded abundant measurement outcomes in wake-related researches. Torres et al. implemented a seven-month LiDAR field campaign to characterize wake interactions between two adjacent wind turbines [5]. Lungo and co-workers deployed three LiDAR instruments to capture wake properties of a 2-MW wind turbine [6]. Meanwhile, Kumer et al. utilized a single LiDAR unit to explore turbulent kinetic energy distribution within turbine wake zones [7].

It should be highlighted that most existing LiDAR-based wake experiments focus on flat-terrain wind-farm scenarios. Few published literatures elaborate on wake evolutionary mechanisms under the combined constraints of incoming-flow characteristics and mountainous topography. Against this research gap, the present work carries out field measurement campaigns at a high-elevation mountain wind farm using two distinct LiDAR devices. Combined with field observation datasets, this paper systematically analyses the separate and coupled influences of terrain and incoming-flow conditions on wake evolution behaviours.

2. Experimental Equipment and Scheme

2.1. LiDAR and Wind Turbine

The field measurement campaign was performed at a mountain-located wind farm featured by complicated landforms, where the mean elevation exceeds 1800 m. To faithfully acquire wake spatial distributions over complex topography, two ground-based coherent Doppler LiDAR instruments of different types were deployed in this test.

The first device is a vertical profiling LiDAR (Model WP350). Its Doppler Beam Swing (DBS) operational mode was adopted to obtain oncoming-flow profiles upstream of the target turbine. The second instrument is a scanning LiDAR (Model 3D6000), which was responsible for wake-field observations. During the experiment, the Range-Height Indicator (RHI) scanning mode was mainly activated, to obtain horizontal-wind-speed contours on the vertical plane behind the turbine rotor through fixed-azimuth vertical pitching scanning.

The tested subject is a 1.5MW wind turbine. Its rotor diameter equals 77 m, hub height is 65 m, and the rated wind speed reaches 12 m/s.

2.2. Wind Measurement Scheme

The layout of measurement instruments is illustrated in Figure 1. The target turbine sits on the northern boundary of the wind farm. No extra turbines exist within 1 km for both upstream and downstream directions, so wake interferences from neighbouring units can be excluded, making this turbine ideal for wake-evolution observations.

Meteorological mast datasets accumulated over the past three years indicate that northwest is the prevailing wind direction of this site. Correspondingly, the WP350 vertical LiDAR was positioned 170 m northwest (upstream) of the target turbine. The 3D6000 scanning LiDAR was placed at a downstream location 1314 m southeast away from the turbine. There exists a 72-m altitude gap between the turbine and the 3D6000 device, which creates favourable conditions for investigating wake evolution subjected to topographic effects.

In order to acquire high-resolution incoming-wind profiles and wake velocity distributions, configuration parameters for LiDAR gates were carefully set. The height gate interval of WP350 was set as 10 m. For 3D6000 scanning LiDAR, its radial gate was set to 20 m and vertical height gate was set to 5 m.

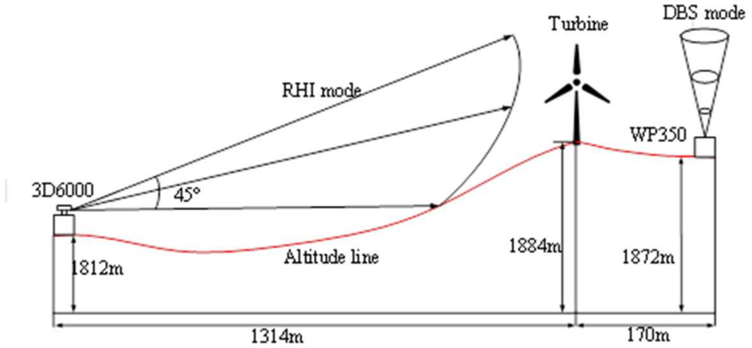

Figure 1. Wind measurement scheme.

3. Experimental Results and Analysis

3.1. Analysis of Wake Characteristics in Vertical Height Plane

Figure 2(a) and Figure 2(b) display horizontal wind-speed contour maps captured on the vertical plane under two separate time instances, and their corresponding incoming-wind vertical profiles are plotted in Figure 3(a) and Figure 3(b), respectively. It should be noted that blank zones in Figure 2 originate from ridge blockage; mountain ridges can obstruct laser beams emitted by LiDAR and disable effective wind-speed acquisition. Nevertheless, such data-missing regions do not prevent us from analysing core wake-field characteristics.

As illustrated in Figure 1, the horizontal axis of Figure 2 corresponds to the connecting line between 3D6000 scanner and target turbine; the turbine is placed at the 1314-m horizontal position, while the vertical axis denotes absolute altitude. Affected by wind-shear effects, incoming wind speed rises as altitude increases for both measured cases.

Compared with condition Figure 3(a), the scenario in Figure 3(b) possesses larger incoming wind speed and higher incoming turbulence intensity, generating more significant wind-shear effects, which follows an approximate exponential distribution. This distribution law agrees well with empirical wind-shear formulas specified within IEC and GL industry standards. Furthermore, because of high-altitude rugged terrain of the test wind farm, the wind-shear magnitude observed in this field test is stronger than values commonly seen on flat-land sites.

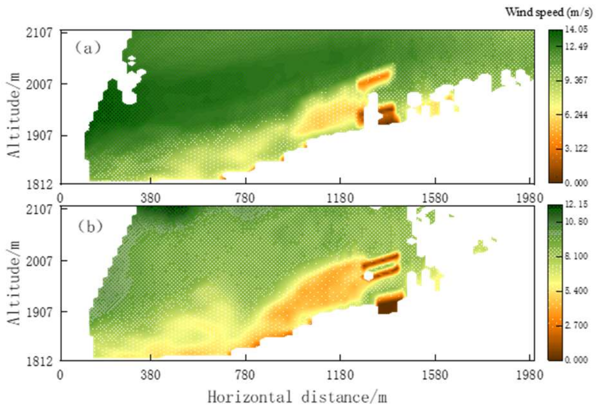

Figure 2. Cloud map of wind speed distribution in the vertical plane.

Subject to wind-shear forcing, wind-speed fields at various downstream distances behind the turbine demonstrate obvious asymmetric features (Figure 2(a)-(b)). In the wake zone, wind speed increases at positions above hub elevation, whereas wind-speed values drop within near-ground regions.

To quantitatively describe vertical-plane wake distributions, wake wind-speed data at multiple downstream cross-sections were extracted for generating wake profile curves, as shown in Figure 3(c) and Figure 3(d). The plots further verify that under two different hub-height inflow conditions, wake velocity fields lose axial symmetry under wind-shear impacts, despite their overall similar distribution patterns.

Within wake core regions, wind-speed magnitudes increase along the upward direction, followed by downward-direction reductions. With growing downstream distance away from the turbine, wake interference effects decay progressively. Beyond 8D downstream (D = 77 m, rotor diameter of the test turbine), wake core signatures fade away gradually, and wake velocity profiles tend to recover toward original incoming-wind profiles.

The underlying physical mechanism can be interpreted as follows. Wind-shear yields exponential growth for incoming wind speed with altitude. Combined with the axisymmetric rotor geometry, wake-region wind fields develop asymmetric distributions. In the upper-hub wake boundary zone, wake wind speed gradually recovers back to incoming-flow magnitudes, and the vertical profile gradually conforms to upstream inflow characteristics.

For areas below the turbine hub, wake velocity distributions become more complicated, jointly governed by rotor blade rotation, tower shadow effect and ground friction. Inside wake boundaries, momentum exchange driven by rotating rotor blades accelerates local wind speed. Outside wake boundaries, weakened momentum exchange together with tower-shadow and ground friction will lead to wind-speed attenuation.

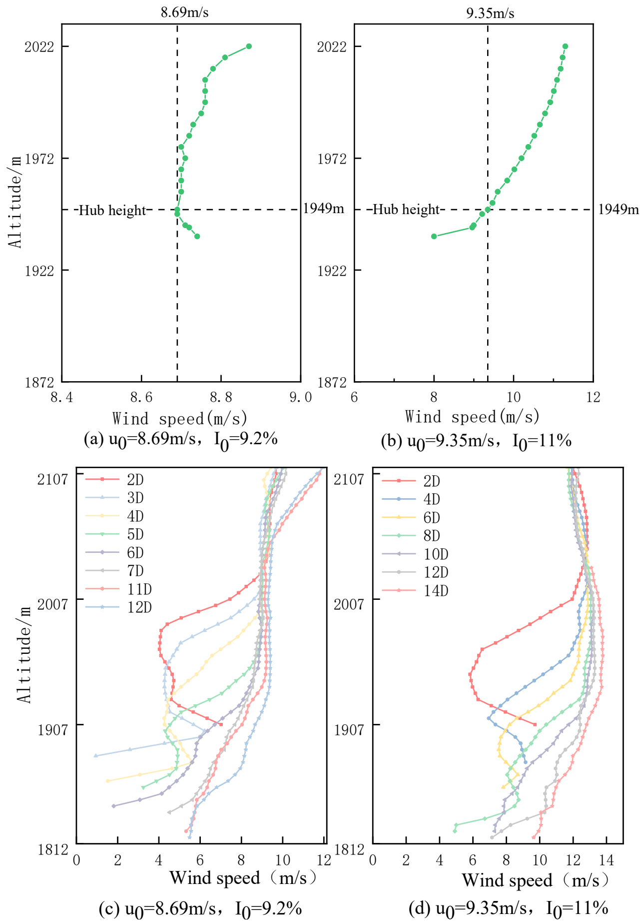

Figure 3. (a) and (b): Incoming wind profile; (c) and (d): Wind speed distribution of vertical plane at different downwind distances.

3.2. Analysis of the Impact of Terrain Effects on Wake Sinking

For wind turbines erected on flat terrain, existing studies confirm that wake core locates roughly at the hub-height elevation. However, for mountain-complex-terrain wind farms with prominent elevation variations, ridge-induced topographic acceleration will force wake core to shift downward, altering spatial patterns of wake wind-speed distribution.

Within this measurement campaign (Figure1), the elevation difference between target turbine and 3D6000 scanner reaches 77 m, with local ridge slope of 10°. From Figure 2 and Figure3, we can clearly observe that wake core drifts downward following the ridge slope direction.

To quantitatively establish the linkage between wake-core downward offset and terrain elevation drop, Figure 4 plots the terrain elevation profile connecting the turbine and downstream LiDAR. The red solid curve represents measured terrain elevation, while the black dashed line is the hypothetical hub-height baseline (shift 65 m upward from raw terrain elevation, corresponding to turbine hub height).

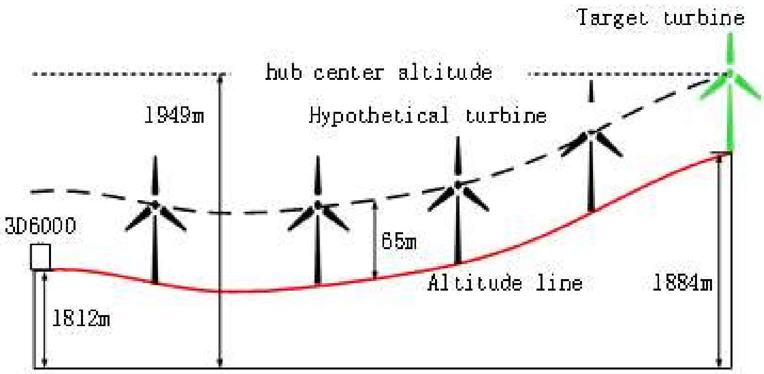

Figure 4. Topographic elevation map.

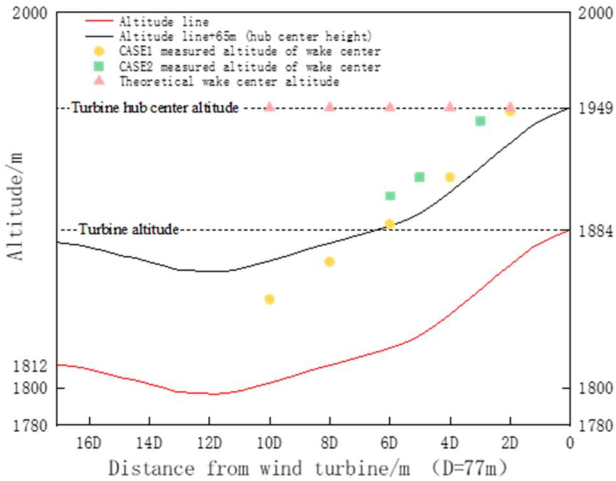

Figure 5. Analysis of the sinking height of the wake center.

Figure 5 compares measured wake-core altitudes, theoretical flat-terrain wake-core altitude and real-world terrain elevation for two independent inflow cases. Dashed lines in the figure mark theoretical wake-core altitude under flat-terrain assumptions.

For CASE 1, wake-core elevations are extracted at 3D, 4D and 5D downstream locations; for CASE 2, data points are collected at 2D, 4D, 6D and 8D downstream positions. These measured wake-core heights are contrasted against theoretical flat-terrain wake-core altitude and hypothetical hub-height reference line.

Comparison results show that as terrain elevation drop (defined as turbine altitude minus local terrain elevation along wake propagation path) increases, wake-core downward-offset magnitudes for CASE1 and CASE2 both increase correspondingly, showing an approximately linear correlation with terrain elevation drop (Figure 6).

For CASE 2, the maximum elevation-derived error emerges at the 10D downstream position, with error magnitude merely 20 m. At the 6D downstream cross-section, measured wake-core downward offset is basically consistent with terrain elevation drop. Although CASE1 only acquires wake-core elevation at three downstream positions, its downward-offset trend is highly consistent with CASE2 observations.

According to above-mentioned experimental analysis, for complex-terrain mountain wind farms, wake-core downward-offset height can be approximately estimated from terrain elevation-drop values.

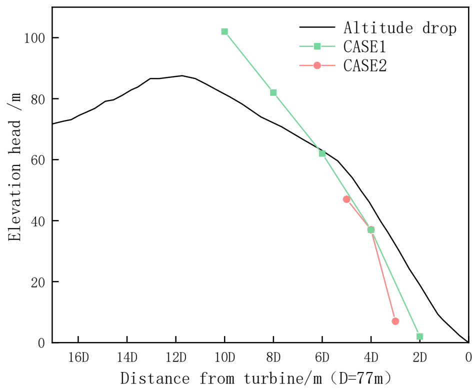

Figure 6. Relationship between the sinking height of the wake center and the altitude drop.

4. Conclusion

This paper implements field measurements for wake characteristics over complex-terrain mountain wind farms, by adopting two categories of LiDAR devices. The influences of wind-shear effect on wake-speed spatial distribution, as well as the correlation between topographic variation and wake-core downward offset are comprehensively analysed. Key conclusions are summarized as follows:

1) Owing to wind-shear influences, wake-region wind-speed fields present obvious asymmetric distribution features. Wind speed rises upward starting from wake core; in the lower-hub zone, tower-shadow effect and ground friction contribute to subsequent wind-speed reduction.

2) Terrain-induced elevation drop triggers wake-core downward migration, and the magnitude of wake-core sinking holds an approximate linear relationship with terrain elevation difference.

3) Under combined coupling effects from wind-shear and mountain topography, wake velocity fields of complex-terrain wind farms exhibit asymmetric spatial distribution. Wake-core position drifts downward following downstream terrain elevation drop. Meanwhile, wake recovery speed is subject to incoming-flow characteristic parameters.

Acknowledgments

This work has received support from the Central South Electric Power Test and Research Institute of China Datang Corporation Science and Technology Research Institute Co., Ltd., for which I would like to express my heartfelt gratitude.

References

[1] Barthelmie, R. J., Hansen, K., Frandsen, S. T., Rathmann, O., Schepers, J. G., Schlez, W., Phillips, J., Rados, K., Zervos, A., Politis, E. S., & Chaviaropoulos, P. K. (2009). Modelling and measuring flow and wind turbine wakes in large wind farms offshore. Wind Energy, 12(5), 431–444. https://doi.org/10.1002/we.348

[2] Wu, Y. T., & Porté-Agel, F. (2012). Atmospheric turbulence effects on wind-turbine wakes: An LES study. Energies, 5(12), 5340–5362. https://doi.org/10.3390/en5125340

[3] Mathew, S. (2006). Wind energy: Fundamentals, resource analysis and economics. Springer.

[4] Gao, X., Li, B., Wang, T., Sun, H., Yang, H., Li, Y., & Zhao, F. (2020). Investigation and validation of 3D wake model for horizontal-axis wind turbines based on field measurements. Applied Energy, 260, 114272. https://doi.org/10.1016/j.apenergy.2019.114272

[5] Iungo, G. V., Wu, Y. T., & Porté-Agel, F. (2013). Field measurements of wind turbine wakes with lidars. Journal of Atmospheric and Oceanic Technology, 30(2), 274–287. https://doi.org/10.1175/JTECH-D-12-00051.1

[6] Torres Garcia, E., Aubrun, S., Coupiac, O., Girard, N., & Boquet, M. (2019). Statistical characteristics of interacting wind turbine wakes from a 7-month LiDAR measurement campaign. Renewable Energy, 130, 1–11. https://doi.org/10.1016/j.renene.2018.06.065

[7] Kumer, V. M., Reuder, J., Dorninger, M., Zauner, R., & Grubišić, V. (2016). Turbulent kinetic energy estimates from profiling wind LiDAR measurements and their potential for wind energy applications. Renewable Energy, 99, 898–910. https://doi.org/10.1016/j.renene.2016.07.014